Supporting Information

Revealing the Reaction Mechanism of Ammonia Synthesis over Bimetallic Nitrides Catalyst from a Kinetic Perspective

Shuairen Qian[1], *Zhengwen Li*[1], *Xiaohang Sun*[1], *Yuxin Chen*[1],
Kai Feng[1,2], *Kaiqi Nie*[1], *Binhang Yan*[1*], *Yi Cheng*[1*]

[1]Department of Chemical Engineering, Tsinghua University, Beijing 100084, P. R. China

[2]Institute of Functional Nano & Soft Materials (FUNSOM), Soochow University, Suzhou, Jiangsu 215123, P. R. China

[*] **Corresponding Author:** Prof. Yi Cheng, E-mail address: yicheng@tsinghua.edu.cn.

Prof. Binhang Yan, E-mail address: binhangyan@tsinghua.edu.cn.

Table of Contents

S1 Research Methods

S1.1 Computational methods

All spin-polarization density functional theory (DFT) calculations were carried out using the Vienna Ab initio Simulation Package (VASP) code with the dispersion effect correction of DFT-D3 method[1,2]. The valence electrons were described by a plane-wave basis set and the interaction between the atomic cores and valence electrons were replaced by projector augmented-wave pseudopotentials[3,4]. The exchange-correlation energies were calculated with the generalized gradient approximation with the Perdew-Burke-Ernzerhof functional (GGA-PBE)[5]. The kinetic cut-off energy was set as 450 eV and the convergence criteria for the electronic steps and ionic steps were set as 10^{-5} eV and 0.03 eV/Å, respectively. The crystal structure model of Co_3Mo_3N (mp-22166) was used for subsequent catalytic reaction studies. Four-layer *p* (2×2) supercells of (111) facet were built as previous reports and the Brillouin zones were sampled by Monkhorst-Pack Γ-points[6–8]. The top two atomic layers were relaxed and a vacuum region of 15 Å was created. The transition states were searched by the climbing-image nudged elastic band (CI-NEB) method and dimer method, and confirmed with vibrational frequency analysis[9,10]. Only one imaginary frequency along the minimum energy path should exist. The adsorption energy of N_xH_y species were defined as:

$$E_{\mathrm{ads}} = E_{\mathrm{ads\_N}_x\mathrm{H}_y} - E_{\mathrm{slab}} - \frac{x}{2}E_{\mathrm{N}_2} - \frac{y}{2}E_{\mathrm{H}_2} \tag{S1}$$

where E_{ads} is adsorption energy of the adsorption species, $E_{\mathrm{ads\_N}_x\mathrm{H}_y}$ is electron energy of the adsorbed intermediate on the surface. E_{slab}, E_{NH_3} and E_{H_2} is electron energy of clean surface, NH_3 gas and H_2 gas, respectively.

Vibrational frequency analysis was performed to calculate the free energy. The zero-point energy (ZPE) correction was defined as:

$$\mathrm{ZPE} = \sum_i \frac{hv_i}{2} \tag{S2}$$

where h is Planck's constant and v_i is the vibrational frequency. The standard internal energy contribution is calculated as:

$$U^o = RT\sum_i \frac{hv_i / k_B}{e^{hv_i/k_BT} - 1} \tag{S3}$$

where k_B is Boltzmann constant and R is gas constant. The standard entropy contribution is given by:

$$S^o = R\sum_i [\frac{hv_i / k_BT}{e^{hv_i/k_BT} - 1} - \ln(1 - e^{hv_i/k_BT})] \tag{S4}$$

and the free energy correction is defined as:

$$G = E + ZPE + \gamma(1 + \ln\frac{p}{p^o}) + U^o - TS^o \tag{S5}$$

where E is the DFT energy, $\gamma = 1$ if the system is gaseous, and $\gamma = 0$ if the system is surface reactant, p is the partial pressure.

The Bader charge was calculated to measure the charge transfer[11,12]. The projected density of states (PDOS) was calculated to understand the electronic structure and the metal d band center was calculated as:

$$\varepsilon_d = \frac{\int_{+\infty}^{+\infty} n_d(\varepsilon)\varepsilon \, d\varepsilon}{\int_{+\infty}^{+\infty} n_d(\varepsilon) \, d\varepsilon} \tag{S6}$$

where ε_d is the d band center. ε is the energy and n is the corresponding density of states.

S1.2 Microkinetic model

The mean-field microkinetic modeling (MKM) was used to measure the reaction rates for Co_3Mo_3N catalyst. The turnover frequency (TOF) can be obtained by solving a set of ordinary differential equations:

$$\frac{\partial \theta_i}{\partial t} = 0 \tag{S7}$$

$$\sum_i \theta_i = 1 \tag{S8}$$

$$r_i = k_i^f \prod_j \theta_{ij} \prod_j p_{ij} - k_i^r \prod_k \theta_{ik} \prod_k p_{ik} \tag{S9}$$

where θ_i is the coverage of the surface species *i* and r_i is the reaction rate of reaction intermediates *i* (i.e. TOF). k_i^f and k_i^r are the forward and reverse rate constants, respectively. The degree of rate control (DRC) analysis was carried out to obtain the information about rate-determining step (RDS)[13–15]. The elementary reactions of catalytic cycle were given in the Section **Reaction mechanism and microkinetic model**.

S1.3 Catalyst preparation

The Co_3Mo_3N catalysts were synthesized by the nitridation of oxide precursors. 2 mmol $(NH_4)_6Mo_7O_{24}\cdot 4H_2O$ (purchased from Sinopharm) and 14 mmol $Co(NO_3)_2\cdot 6H_2O$ (purchased from Aladdin) were dissolved in 180 mL deionized water and mixed for 10 min. Then the mixture was hydrothermally synthesized at 160 °C for 6 h. The sample was washed with deionized water for three times and then dried at 80 °C overnight. The sample was calcinated at 450 °C for 4 h in air to obtain $CoMoO_4$ precursor and subsequently ammonized at 850 °C for 3 h under N_2/H_2 atmosphere with a ramping rate of 10 $°C\cdot min^{-1}$. The sample was cooled down to room temperature under N_2 gas and passivated in air for 12 h. N_2 (99.99%), H_2 (99.99%), and Ar (99.99%) were purchased from Beijing Huanyu Jinghui Gas Technology Co.

S1.4 Catalyst performance test

The catalyst performance test was carried out in a fixed-bed reactor under atmospheric pressure. Typically, 100 mg catalyst (40–60 mesh) was loaded into a quartz tube with an inner diameter of 4 mm and fixed by quartz wool. Then the catalyst was pretreated at 600 °C for 1 h under N_2/H_2 gas mixture (10 mL·min^{-1} N_2 and 30 mL·min^{-1} H_2) to remove the oxide overlayer. Then the reactor was cooled to reaction temperature to perform the reactivity tests. The kinetic data was collected under 450 °C. The catalytic performance was far from thermodynamic equilibrium under this condition. The output gas was introduced into a diluted H_2SO_4 solution (1 mmol/L) and the ion conductivity was monitored by a conductivity meter (Mettler Toledo SevenMulti) to quantify ammonia production. The quantitative method was the same as the previous literatures[16,17].

S1.5 Catalyst characterization

Phase analysis was identified by X-ray diffraction (XRD, D8 Advance equipped with Cu Kα radiation). The diffraction data was collected between 5° and 90° at a rate of 5°·min^{-1}. Images and element distribution of the catalyst morphology were obtained by high-resolution transmission electron microscopy (HR-TEM, JSM2010, at 200 keV).

S1.6 Temperature-programmed experiments

All temperature-programmed experiments were carried out in a fixed-bed reactor, and the outlet gas was detected online by Fourier transform infrared (FTIR) spectrometer (Thermo Nicolet iS50). Typically, 50 mg catalyst (40–60 mesh) was loaded into a quartz tube with an inner diameter of 4 mm and fixed by quartz wool. Then the catalyst was pretreated at 600 °C for 1 h under N_2/H_2 gas mixture (5 mL·min^{-1} N_2 and 15 mL·min^{-1} H_2) to remove the oxide overlayer. The reactor was cooled to room temperature and purged with 20 mL·min^{-1} of Ar gas for 30 min. Then the inlet gas was switched to reaction gas and the reactor was heated to 700 °C with a ramping rate of 10 °C·min^{-1} and kept for 30 min.

S1.7 Steady-state isotopic-transient kinetic analysis (SSITKA)

The steady-state isotopic transient kinetic analysis (SSITKA) experiment was performed in a home-built experimental system. Typically, 50 mg catalyst (40–60 mesh) was loaded into a quartz tube with an inner diameter of 4 mm and fixed by quartz wool. Then the catalyst was pretreated at 600 °C for 1 h under N_2/H_2 gas mixture (5 $mL·min^{-1}$ N_2 and 15 $mL·min^{-1}$ H_2) to remove the oxide overlayer. Then the reactor was cooled to reaction temperature. Steady-state ammonia synthesis was performed for 30 min under $N_2/H_2/Ar$ gas mixture (5 $mL·min^{-1}$ N_2, 15 $mL·min^{-1}$ H_2 and 10 $mL·min^{-1}$ Ar). The reaction gas was instantaneously switched to isotopic gas (5 $mL·min^{-1}$ $^{15}N_2$, 15 $mL·min^{-1}$ H_2 and 10 $mL·min^{-1}$ Kr). the outlet gas was detected online by high time-resolution mass spectrometry (Hiden QGA).

S2 DFT Calculation Screening and Testing

S2.1 Calculation Tests

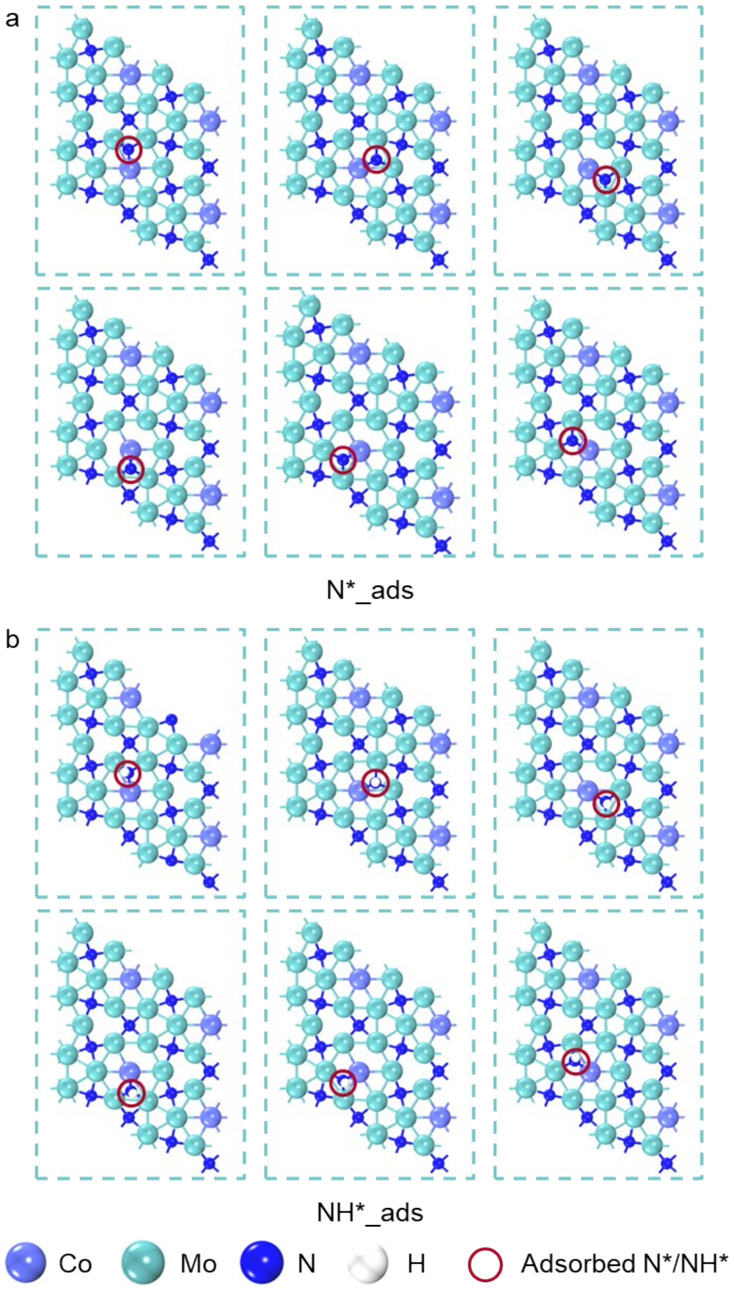

Figure S1 Schematic structures of (a) N* adsorption and (b) NH* adsorption for different CoMo2 sites. The red circle represents the position of the adsorbed N.

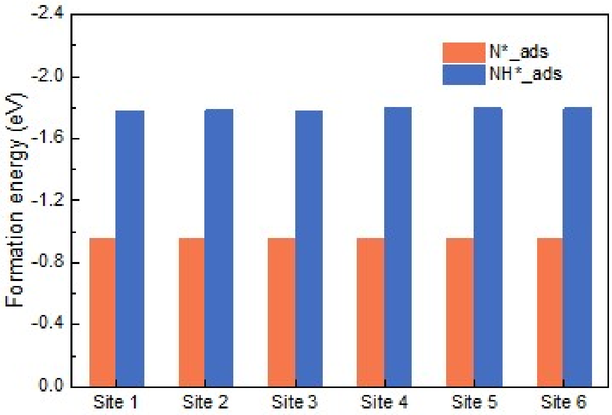

Figure S2 Formation energy of adsorbed species for different CoMo2 sites.

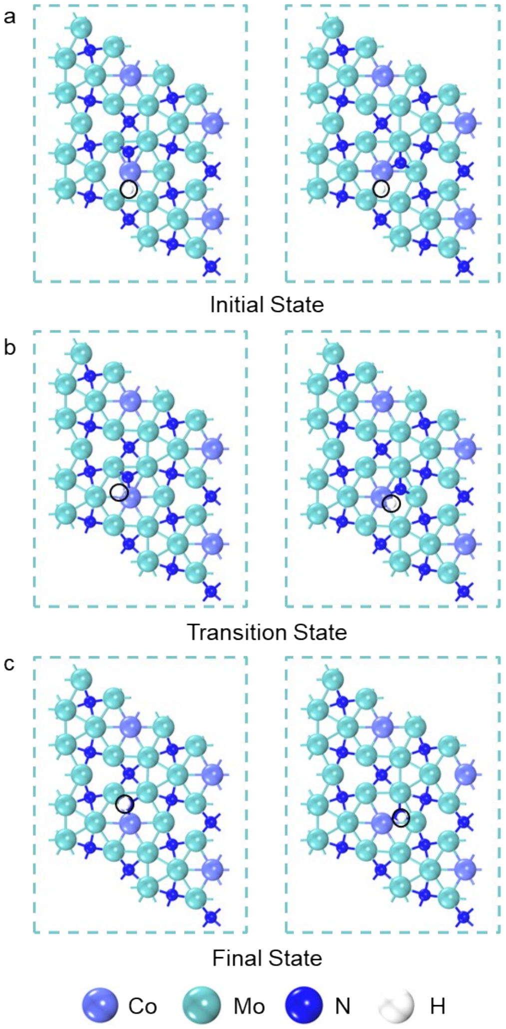

Figure S3 Schematic structures of (a) initial state of N* and H*, (b) transition state and (c) final state of NH* for different CoMo2 sites. The black circle represents the position of the adsorbed H.

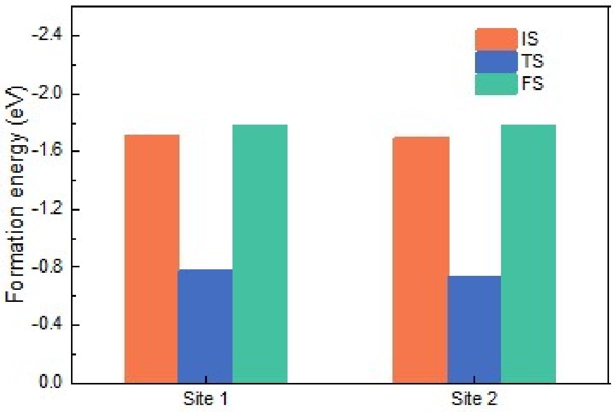

Figure S4 Formation energy of transition state search for different CoMo2 sites.

Supplementary Notes

The CoMo6 ensemble on the Co_3Mo_3N surface consists of six CoMo2 sites. In order to locate where the catalytic reaction takes place, the DFT convergence tests were performed. Specifically, adsorption energies and transition state energies were calculated for six CoMo2 sites. Almost identical energies were obtained for these sites, indicating that these sites are completely equivalent and that any one of them can be selected for subsequent studies.

S2.2 Adsorption configuration screening

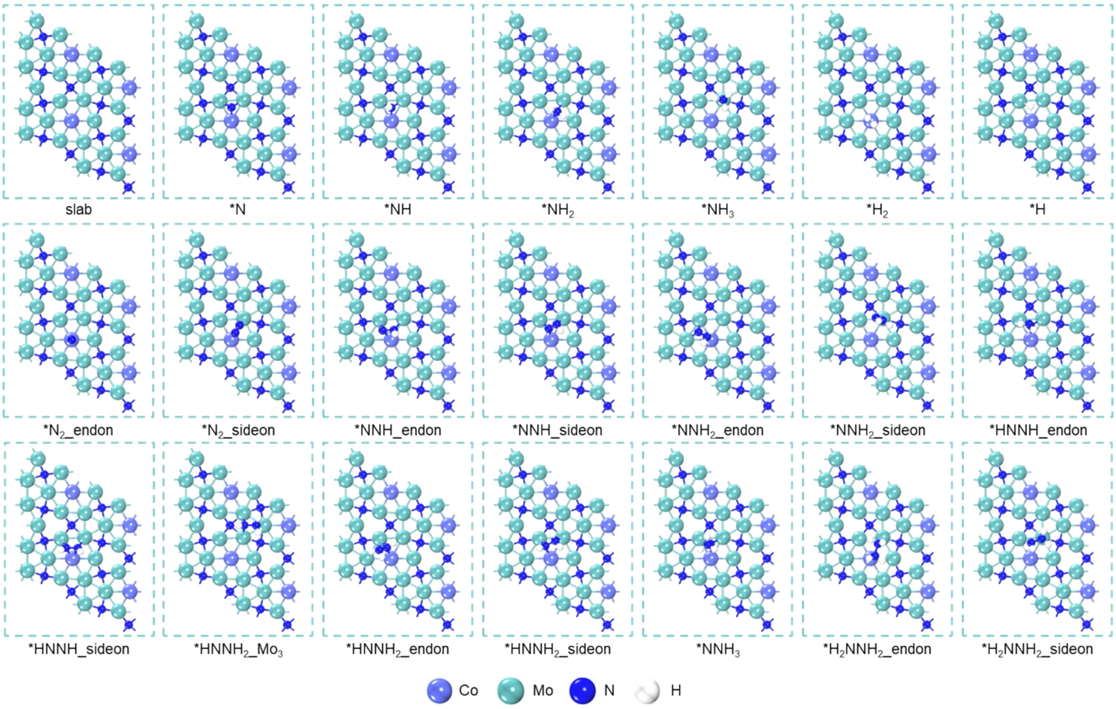

Figure S5 Schematic structures of optimal adsorption configuration.

Table S1 The summary of the adsorption energy corresponding to the adsorption configuration.

Adsorption species	**Site**	E_{ads} **(eV)**
H	hollow_CoMo2	-0.65
N	hollow_CoMo2	-0.95
NH	hollow_CoMo2	1.14
NH_2	bri_CoMo	0.63
NH_3	top_Mo	0.53
N_2	sideon_bri_CoMo	-0.98
NNH	sideon_hollow_CoMo2	1.45
NNH_2	sideon_hollow_CoMo2	1.34
NNH_3	endon_hollow_CoMo2	1.94
HNNH	sideon_hollow_CoMo2	1.23
$HNNH_2$	sideon_hollow_Mo3	0.72
H_2NNH_2	sideon_bri_CoMo	1.22

S3 Reaction Mechanism And Microkinetic Model

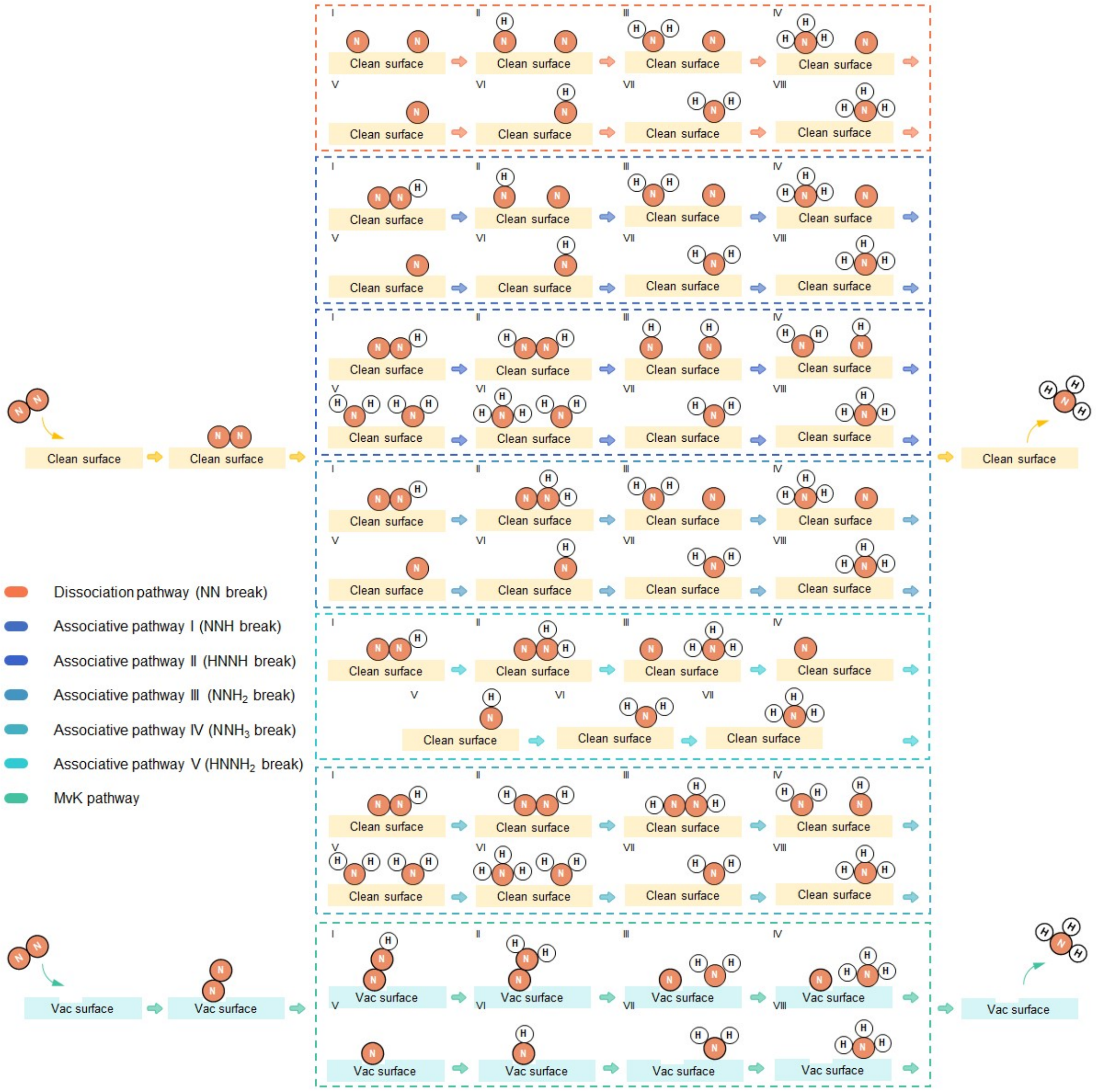

Figure S6 Schematic depiction of the reaction mechanisms for ammonia synthesis.

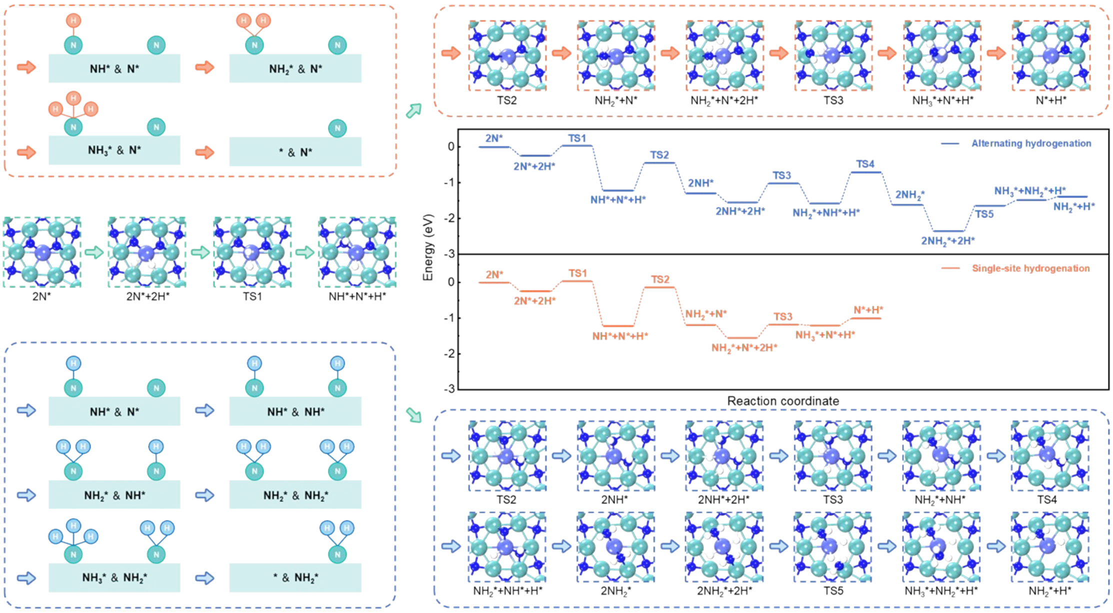

Figure S7 The energy test for alternating hydrogenation and single-site hydrogenation.

Supplementary Notes

When N_2 dissociation occurs on the surface, two separate N atoms are produced. When hydrogenation occurs, there are two types of hydrogenation modes, namely, single-site (preferential addition of H to one N atom) and alternating (alternating hydrogenation of two N atoms). According to the calculated potential energy profile, single-site hydrogenation is energetically more favorable. Therefore, single-site hydrogenation is considered in this work.

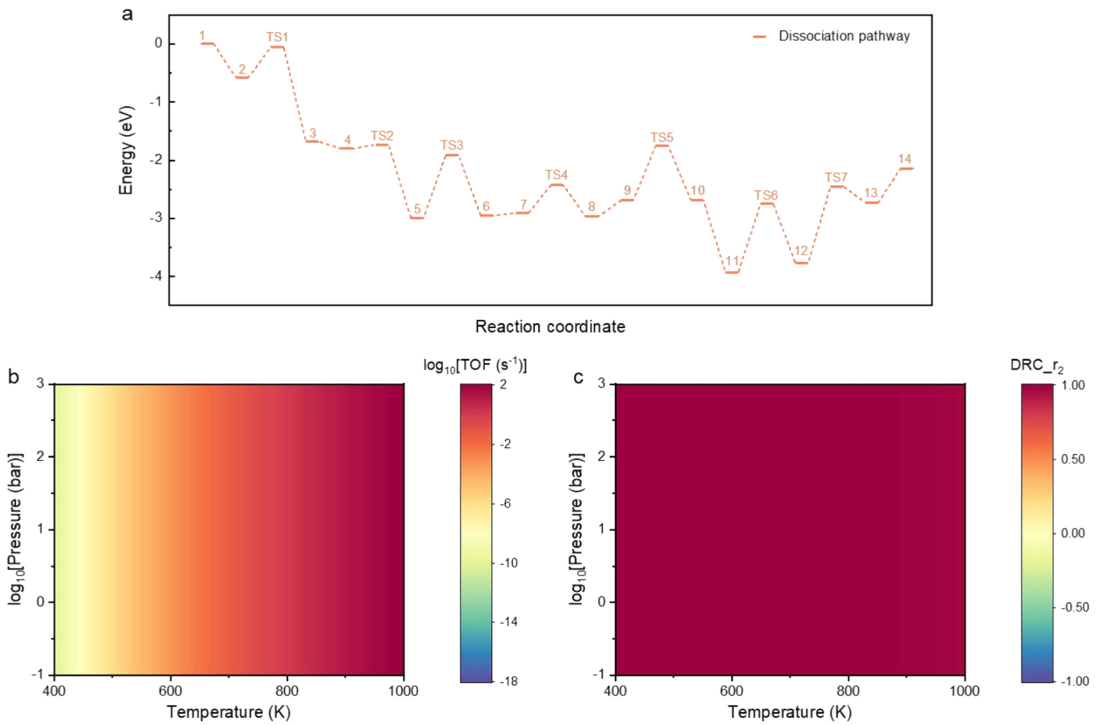

Figure S8 (a) Calculated potential energy profile of NH_3 synthesis for Co_3Mo_3N catalyst via dissociation pathway and corresponding (b) microkinetic reaction rate heatmap and (c) DRC analysis at $N_2/H_2 = 1/3$.

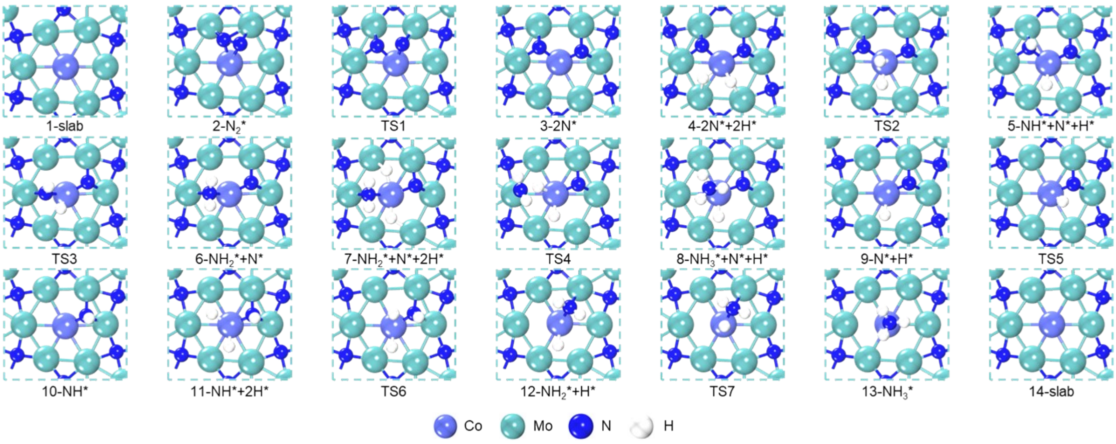

Figure S9 Schematic structures of the optimized intermediate species for dissociation pathway.

Table S2 The DFT energetics of dissociation pathway.

No.	Elementary reaction	Barrier (eV)	Heat (eV)
1	N_2_g + *_s -> N_2*	-	-0.58
2	H_2* + 2*_s -> 2H*	-	-1.43
3	N_2* + *_s <-> N-N* + *_s -> 2N*	0.53	-1.32
4	N* + H* <-> N-H* + *_s -> NH* + *_s	0.99	0.06
5	NH* + H* <-> NH-H* + *_s -> NH_2* + *_s	1.15	0.33
6	NH_2* + H* <-> NH_2-H* + *_s -> NH_3* + *_s	1.33	1.05
7	NH_3* -> NH_3_g + *_s	0.59	0.59

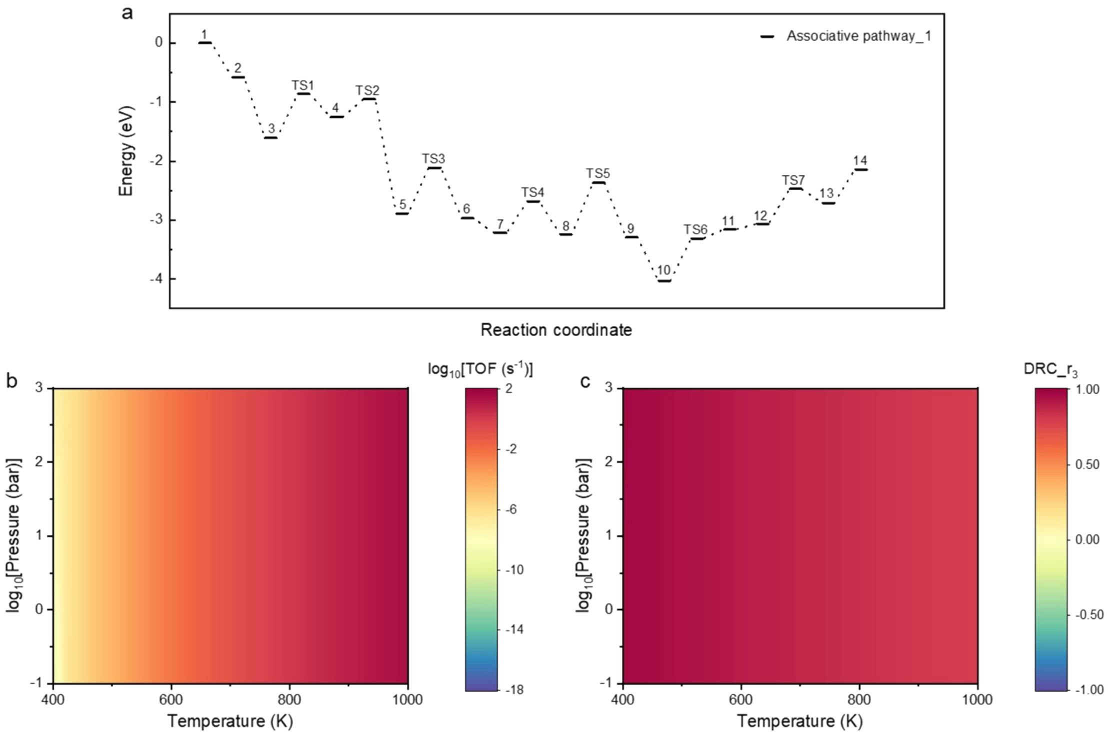

Figure S10 (a) Calculated potential energy profile of NH_3 synthesis for Co_3Mo_3N catalyst via associative pathway I and corresponding (b) microkinetic reaction rate heatmap and (c) DRC analysis at $N_2/H_2 = 1/3$.

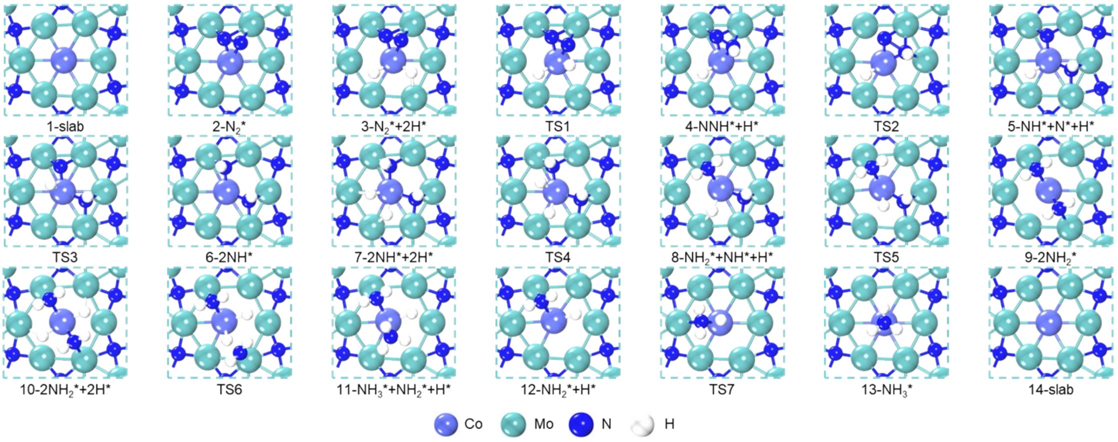

Figure S11 Schematic structures of the optimized intermediate species for associative pathway I.

Table S3 The DFT energetics of associative pathway I.

No.	Elementary reaction	Barrier (eV)	Heat (eV)
1	N_2_g + *_s -> N_2*	-	-0.58
2	H_2* + 2*_s -> 2H*	-	-1.43
3	N_2* + H* <-> N_2-H* + *_s -> NNH* + *_s	1.04	0.67
4	NNH* + *_s <-> NH-N* + *_s -> NH* + N*	0.25	-1.94
4	N* + H* <-> N-H* + *_s -> NH* + *_s	0.99	0.06
5	NH* + H* <-> NH-H* + *_s -> NH_2* + *_s	1.15	0.33
6	NH_2* + H* <-> NH_2-H* + *_s -> NH_3* + *_s	1.33	1.05

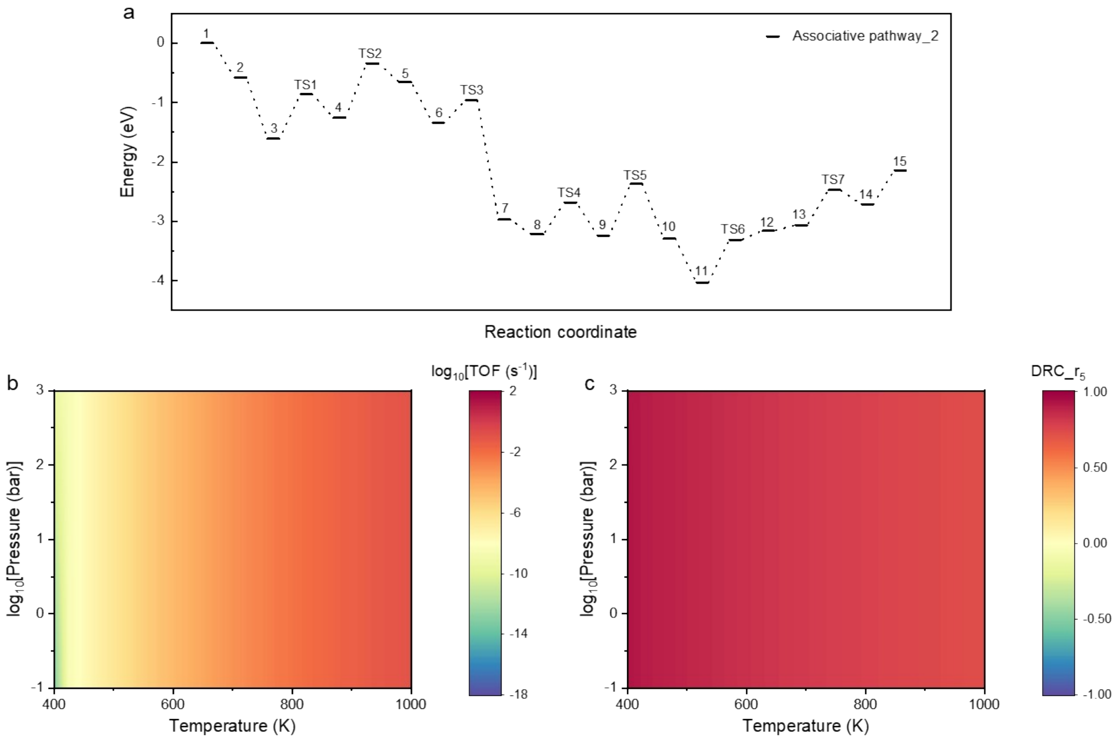

Figure S12 (a) Calculated potential energy profile of NH_3 synthesis for Co_3Mo_3N catalyst via associative pathway II and corresponding (b) microkinetic reaction rate heatmap and (c) DRC analysis at N_2/H_2 = 1/3.

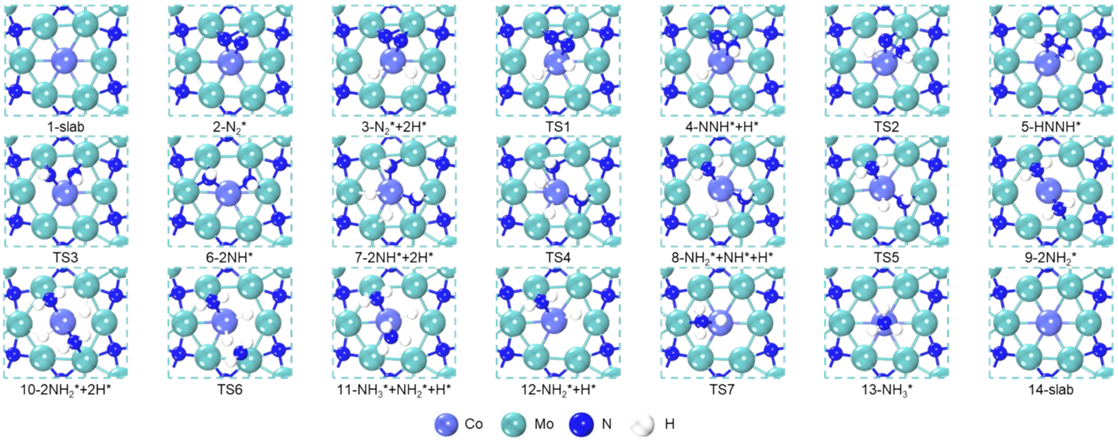

Figure S13 Schematic structures of the optimized intermediate species for associative pathway II.

Table S4 The DFT energetics of associative pathway II.

No.	Elementary reaction	Barrier (eV)	Heat (eV)
1	N_2_g + *_s -> N_2*	-	-0.58
2	H_2* + 2*_s -> 2H*	-	-1.43
3	N_2* + H* <-> N_2-H* + *_s -> NNH* + *_s	1.04	0.67
4	NNH* + H* <-> NNH-N* + *_s -> HNNH*	1.00	0.68
5	HNNH* + *_s <-> HN-NH* + *_s -> 2NH*	0.41	-1.84
6	NH* + H* <-> NH-H* + *_s -> NH_2* + *_s	1.15	0.33
7	NH_2* + H* <-> NH_2-H* + *_s -> NH_3* + *_s	1.33	1.05
8	NH_3* -> NH_3_g + *_s	0.59	0.59

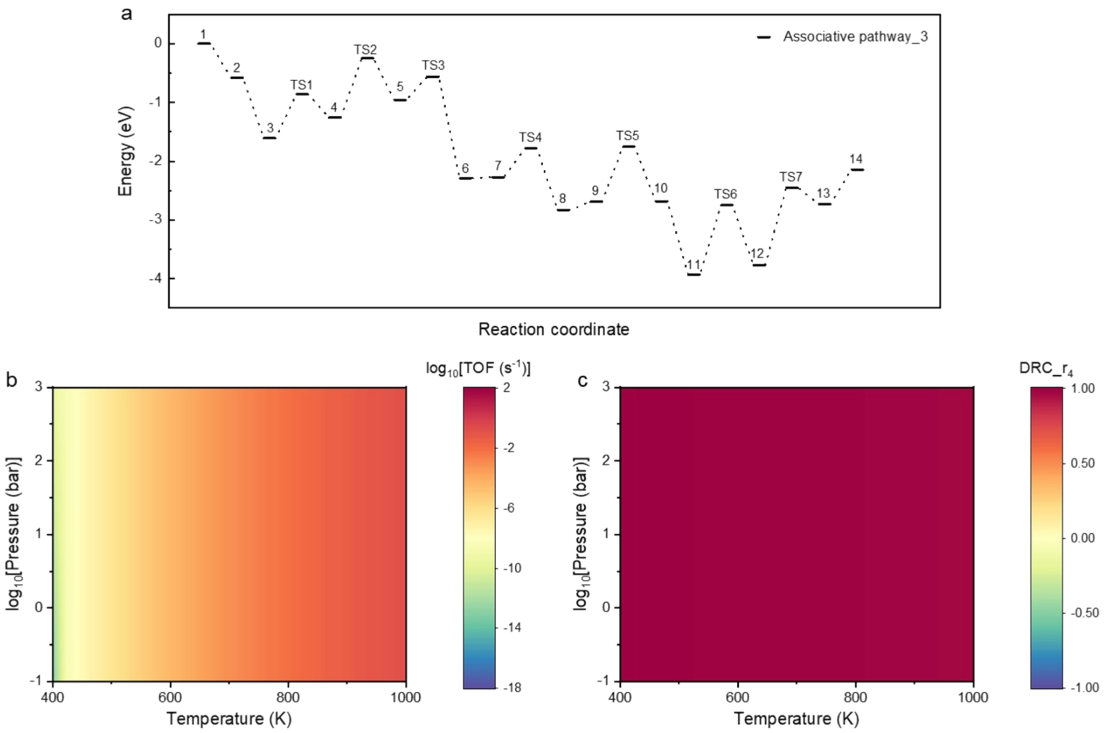

Figure S14 (a) Calculated potential energy profile of NH_3 synthesis for Co_3Mo_3N catalyst via associative pathway III and corresponding (b) microkinetic reaction rate heatmap and (c) DRC analysis at $N_2/H_2 = 1/3$.

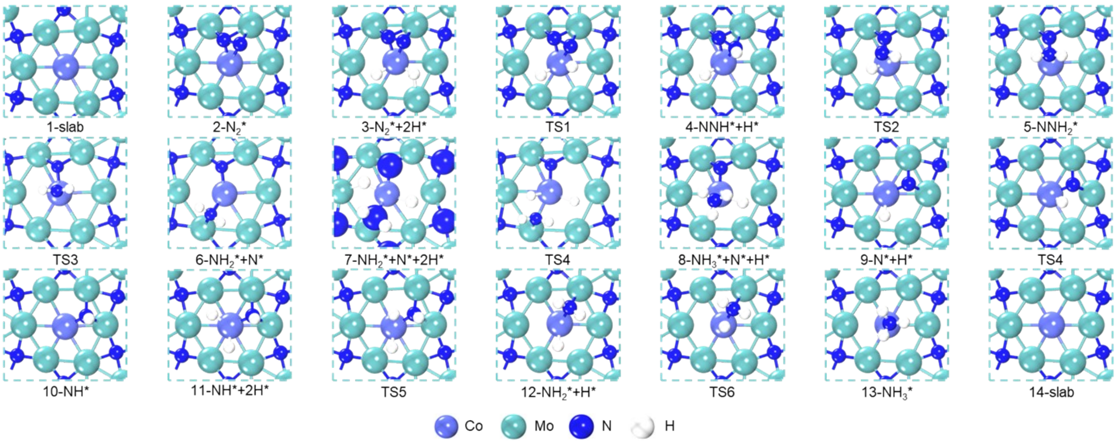

Figure S15 Schematic structures of the optimized intermediate species for associative pathway III.

Table S5 The DFT energetics of associative pathway III.

No.	Elementary reaction	Barrier (eV)	Heat (eV)
1	N_2_g + *_s -> N_2*	-	-0.58
2	H_2* + 2*_s -> 2H*	-	-1.43
3	N_2* + H* <-> N_2-H* + *_s -> NNH* + *_s	1.04	0.67
4	NNH* + H* <-> NNH-N* + *_s -> NNH_2* + *_s	1.09	0.38
5	NNH_2* + * -> N-NH_2* + *_s -> NH_2* + N*	0.39	-1.98
6	N* + H* <-> N-H* + *_s -> NH* + *_s	0.99	0.06
7	NH* + H* <-> NH-H* + *_s -> NH_2* + *_s	1.15	0.33
8	NH_2* + H* <-> NH_2-H* + *_s -> NH_3* + *_s	1.33	1.05
9	NH_3* -> NH_3_g + *_s	0.59	0.59

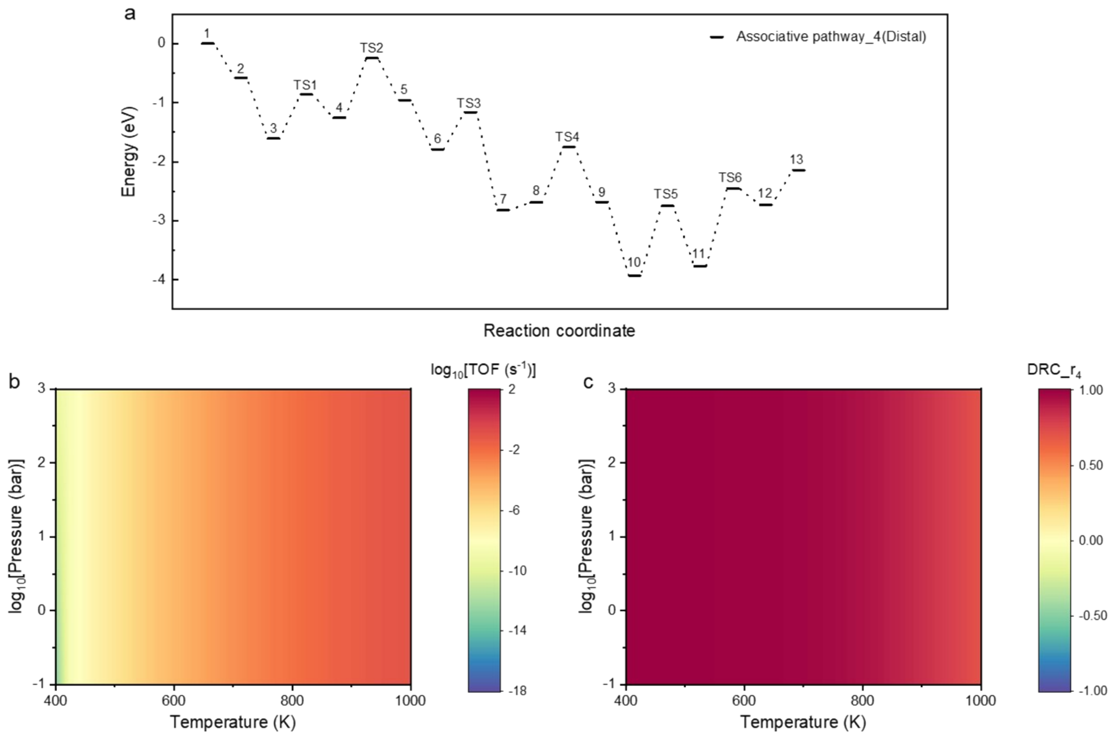

Figure S16 (a) Calculated potential energy profile of NH_3 synthesis for Co_3Mo_3N catalyst via associative pathway IV and corresponding (b) microkinetic reaction rate heatmap and (c) DRC analysis at $N_2/H_2 = 1/3$.

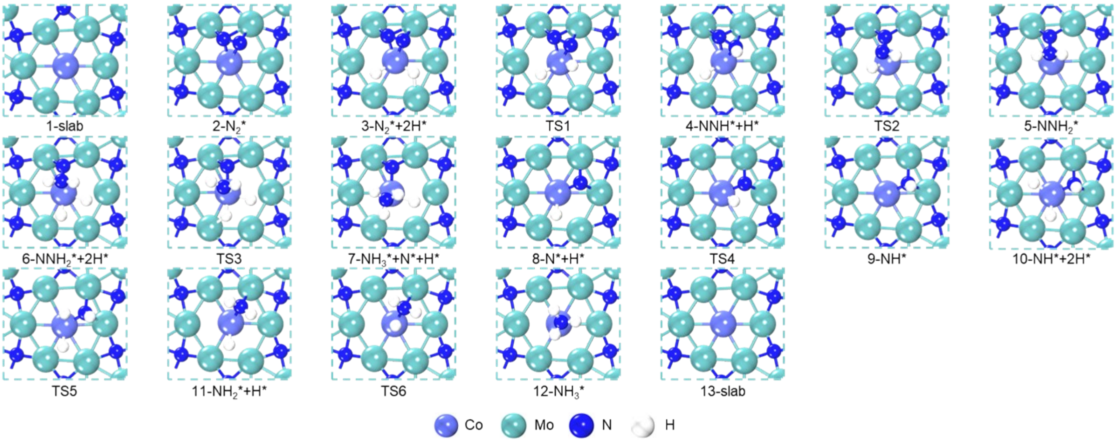

Figure S17 Schematic structures of the optimized intermediate species for associative pathway IV.

Table S6 The DFT energetics of associative pathway IV.

No.	Elementary reaction	Barrier (eV)	Heat (eV)
1	N_2_g + *_s -> N_2*		-0.58
2	H_2* + 2*_s -> 2H*		-1.43
3	N_2* + H* <-> N_2-H* + *_s -> NNH* + *_s	1.04	0.67
4	NNH* + H* <-> NNH-N* + *_s -> NNH_2* + *_s	1.09	0.38
5	NNH_2* + H* -> N-NH_2-H* + *_s -> NH_3* + N*	0.88	-1.02
6	N* + H* <-> N-H* + *_s -> NH* + *_s	0.99	0.06
7	NH* + H* <-> NH-H* + *_s -> NH_2* + *_s	1.15	0.33
8	NH_2* + H* <-> NH_2-H* + *_s -> NH_3* + *_s	1.33	1.05
9	NH_3* -> NH_3_g + *_s	0.59	0.59

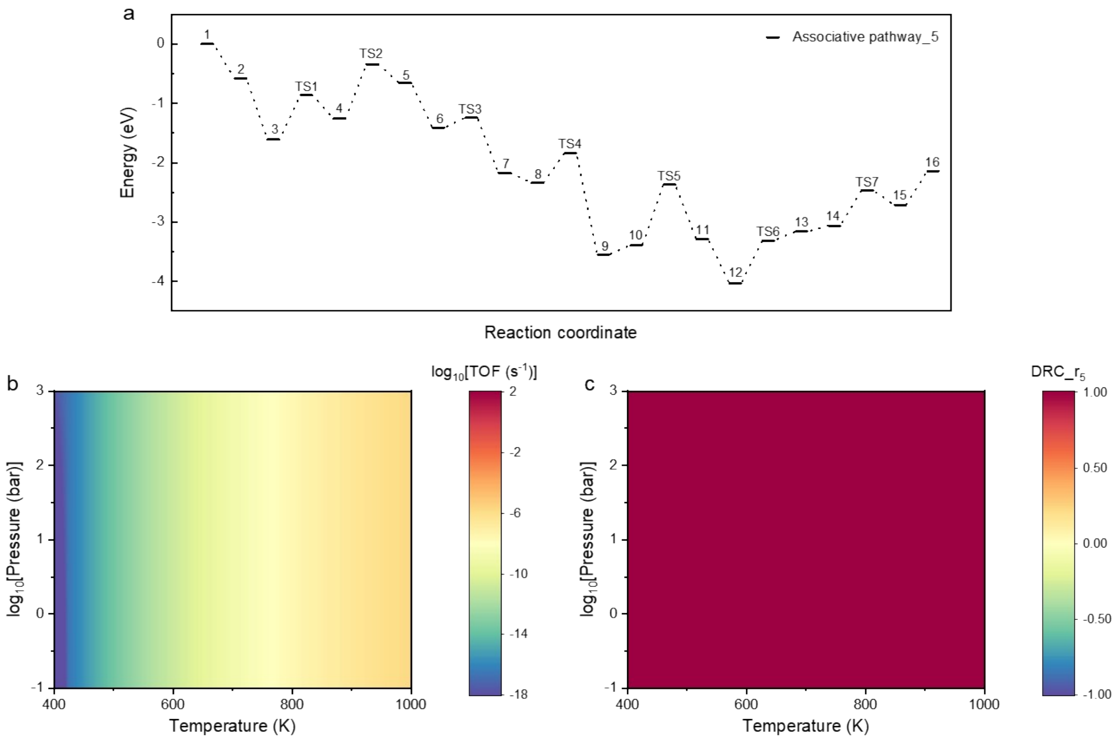

Figure S18 (a) Calculated potential energy profile of NH_3 synthesis for Co_3Mo_3N catalyst via associative pathway V and corresponding (b) microkinetic reaction rate heatmap and (c) DRC analysis at $N_2/H_2 = 1/3$.

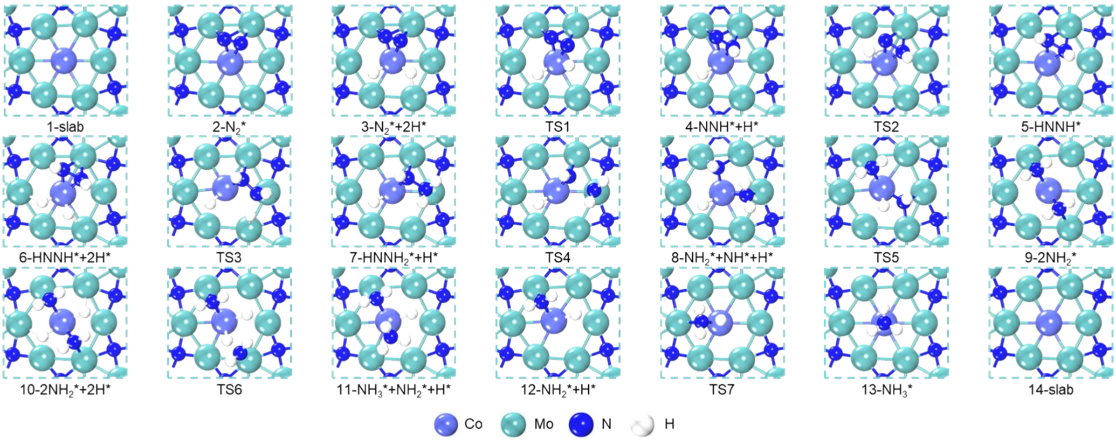

Figure S19 Schematic structures of the optimized intermediate species for associative pathway V.

Table S7 The DFT energetics of associative pathway V.

No.	Elementary reaction	Barrier (eV)	Heat (eV)
1	N_2_g + *_s -> N_2*		-0.58
2	H_2* + 2*_s -> 2H*		-1.43
3	N_2* + H* <-> N_2-H* + *_s -> NNH* + *_s	1.04	0.67
4	NNH* + H* <-> NNH-N* + *_s -> HNNH*	1.00	0.68
5	HNNH* + H* <-> HNNH-H* + *_s -> $HNNH_2$* + *_s	0.88	-1.02
6	$HNNH_2$* + *_s <-> HN-NH_2* + *_s -> NH* + NH_2*	0.46	-2.18
7	NH* + H* <-> NH-H* + *_s -> NH_2* + *_s	1.15	0.33
8	NH_2* + H* <-> NH_2-H* + *_s -> NH_3* + *_s	1.33	1.05
9	NH_3* -> NH_3_g + *_s	0.59	0.59

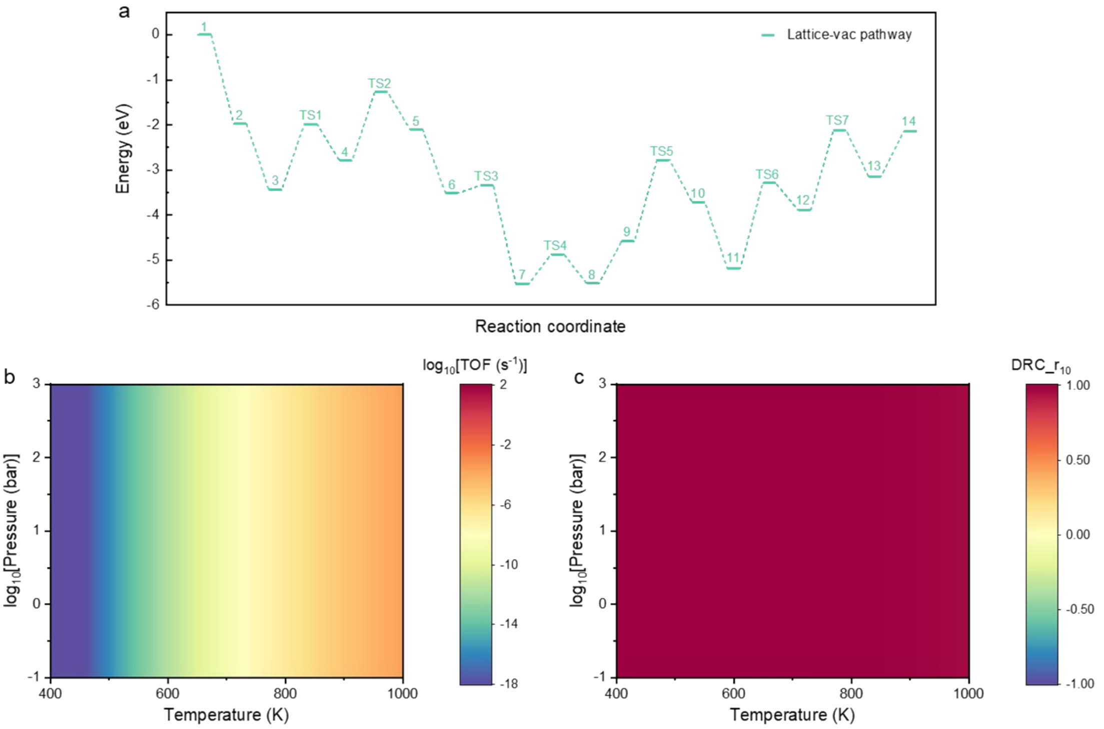

Figure S20 (a) Calculated potential energy profile of NH_3 synthesis for Co_3Mo_3N catalyst via MvK pathway and corresponding (b) microkinetic reaction rate heatmap and (c) DRC analysis at $N_2/H_2 = 1/3$.

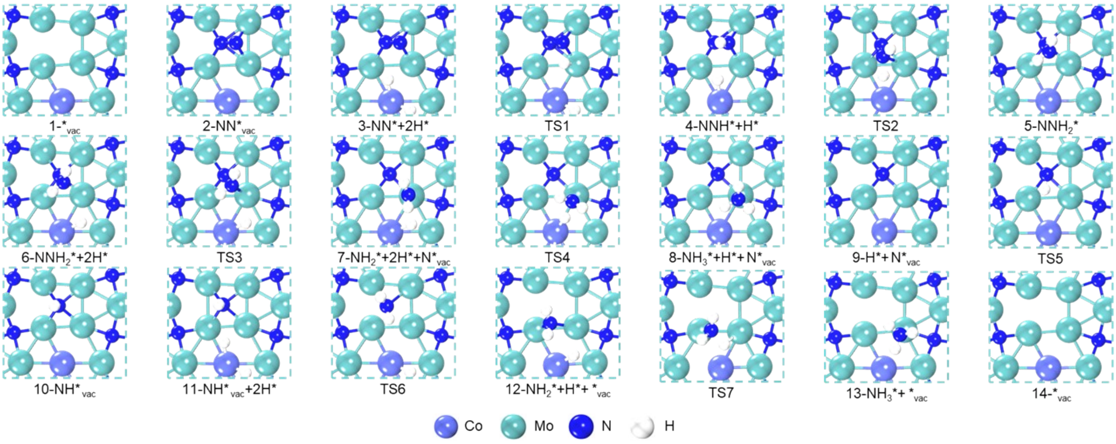

Figure S21 Schematic structures of the optimized intermediate species for MvK pathway.

Table S8 The DFT energetics of MvK pathway.

No.	Elementary reaction	Barrier (eV)	Heat (eV)
1	N_2_g + *_s -> N_2*	-	-0.58
2	H_2* + 2*_s -> 2H*	-	-1.43
3	N_2* + H* <-> N_2-H* + *_s -> NNH* + *_s	1.04	0.67
4	NNH* + H* <-> NNH-N* + *_s -> HNNH*	1.00	0.68
5	HNNH* + H* <-> HNNH-H* + *_s -> $HNNH_2$* + *_s	0.88	-1.02
6	$HNNH_2$* + *_s <-> HN-NH_2* + *_s -> NH* + NH_2*	0.46	-2.18
7	NH* + H* <-> NH-H* + *_s -> NH_2* + *_s	1.15	0.33
8	NH_2* + H* <-> NH_2-H* + *_s -> NH_3* + *_s	1.33	1.05
9	NH_3* -> NH_3_g + *_s	0.59	0.59

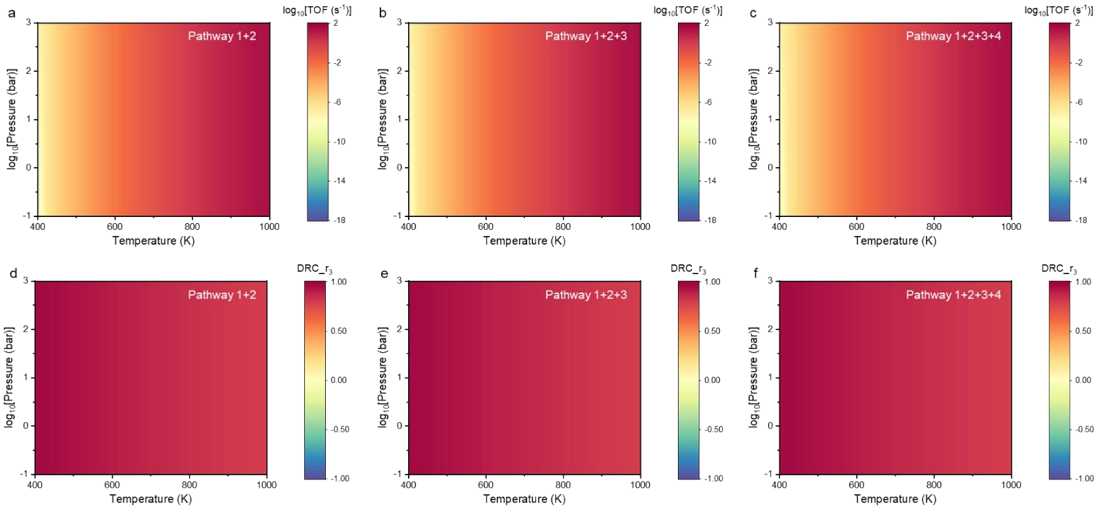

Figure S22 Ammonia synthesis rate (TOF) as a function of temperature and pressure at $N_2/H_2 = 1/3$ for Co_3Mo_3N catalyst via (a) mixing pathway of associative pathway I and II, (b) mixing pathway of associative pathway I, II and III, (c) mixing pathway of associative pathway I, II, III and IV. DRC analysis for (d) mixing pathway of associative pathway I and II, (e) mixing pathway of associative pathway I, II and III, (f) mixing pathway of associative pathway I, II, III and IV.

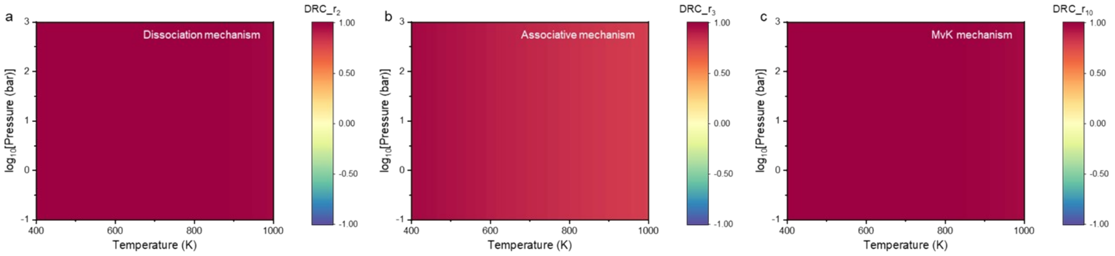

Figure S23 Ammonia synthesis rate (TOF) as a function of temperature and pressure at $N_2/H_2 = 1/3$ for Co_3Mo_3N catalyst via (a) dissociation mechanism, (b) associative mechanism and (c) MvK mechanism.

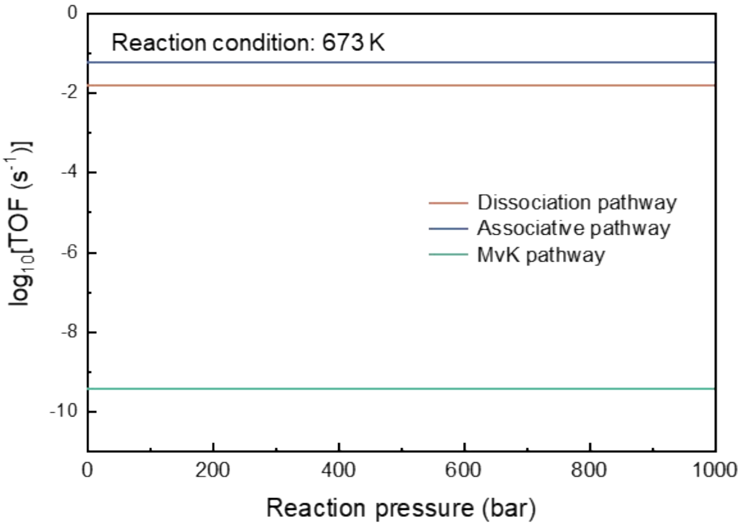

Figure S24 Ammonia synthesis rate for different reaction mechanisms as a function of pressure at 675 K and $N_2/H_2 = 1/3$.

S4 Electronic Structure Analysis

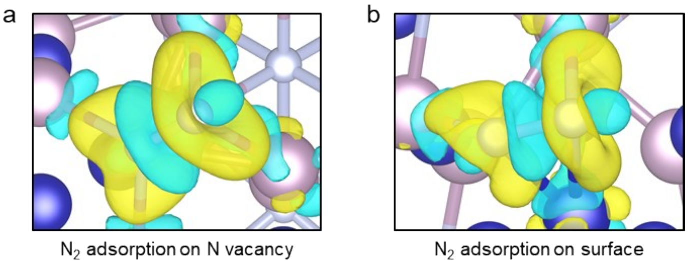

N_2 adsorption on N vacancy

N_2 adsorption on surface

Figure S25 Top view of charge density difference for (a) N_2 adsorption on N vacancy and (b) N_2 adsorption on surface.

S5 Catalyst Characterization

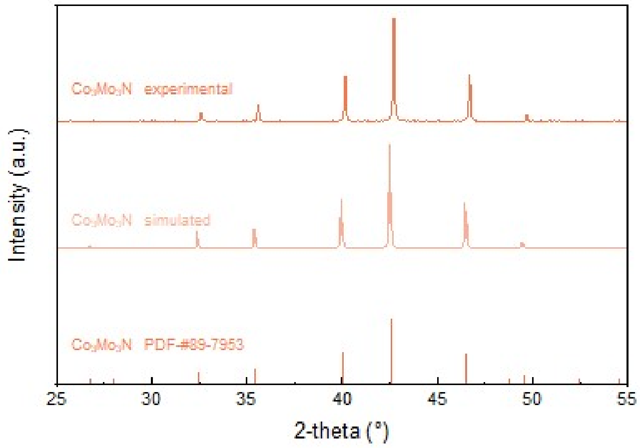

Figure S26 The XRD patterns of Co_3Mo_3N sample.

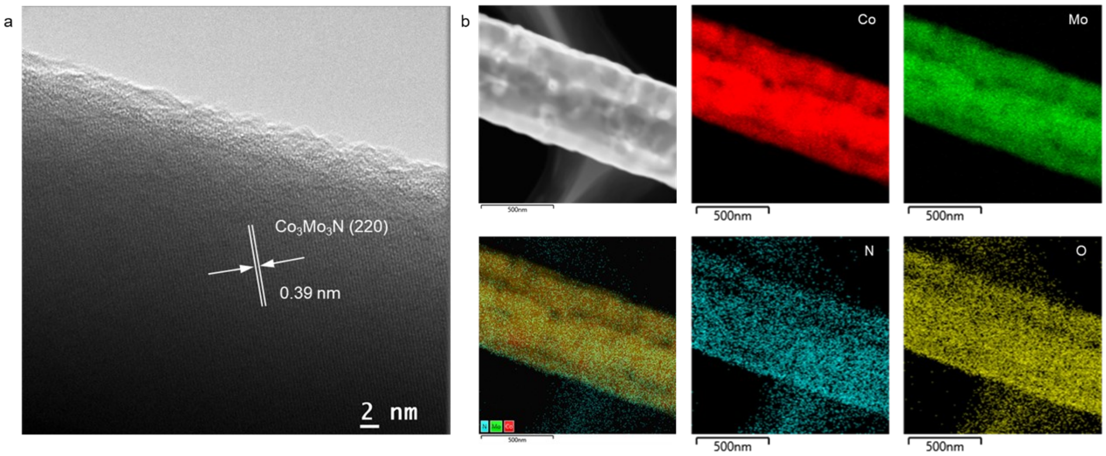

Figure S27 (a) The images of high-resolution transmission electron microscopy (HR-TEM) for Co_3Mo_3N catalyst. (b) Energy-dispersive spectroscopy (EDS) elemental mapping for Co_3Mo_3N catalyst.

S6 Steady-state Kinetic Analysis

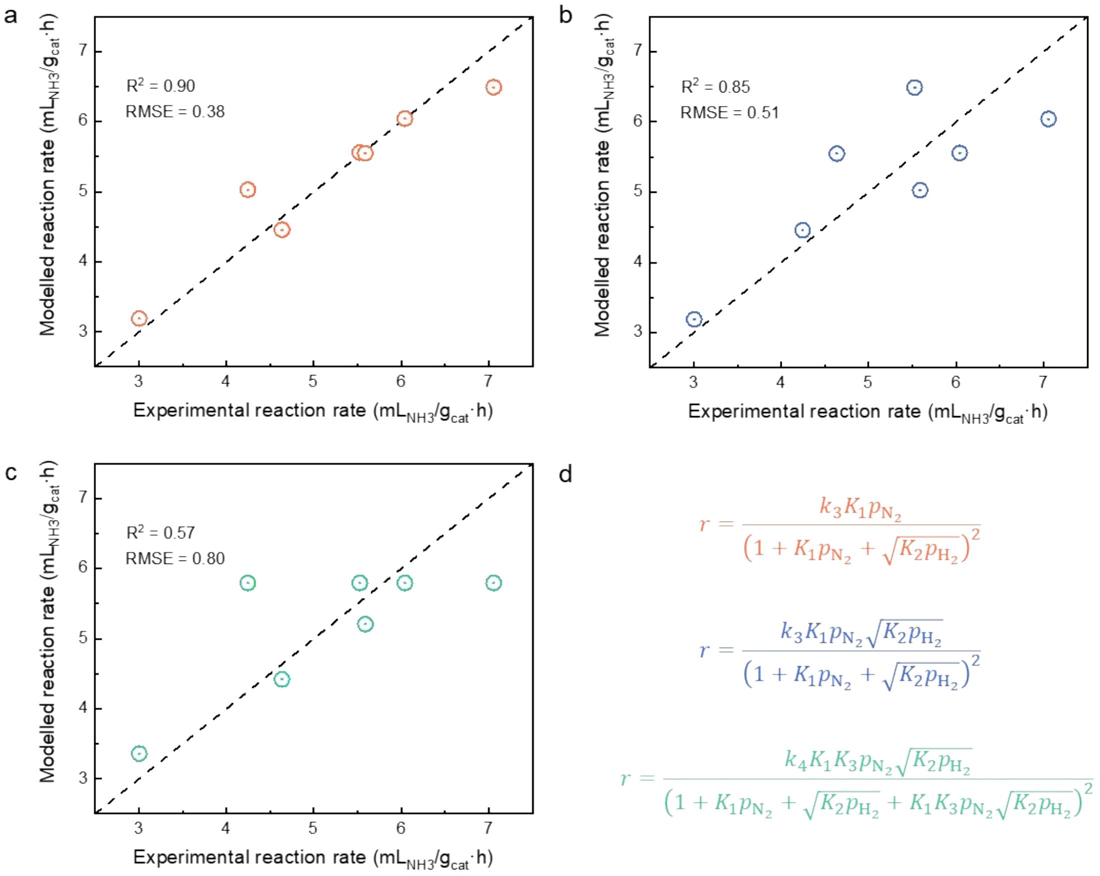

$$r = \frac{k_3 K_1 p_{N_2}}{\left(1 + K_1 p_{N_2} + \sqrt{K_2 p_{H_2}}\right)^2}$$

$$r = \frac{k_3 K_1 p_{N_2} \sqrt{K_2 p_{H_2}}}{\left(1 + K_1 p_{N_2} + \sqrt{K_2 p_{H_2}}\right)^2}$$

$$r = \frac{k_4 K_1 K_3 p_{N_2} \sqrt{K_2 p_{H_2}}}{\left(1 + K_1 p_{N_2} + \sqrt{K_2 p_{H_2}} + K_1 K_3 p_{N_2} \sqrt{K_2 p_{H_2}}\right)^2}$$

Figure S28 Kinetic fit results of reaction rates for (a) dissociation pathway, (b) associative pathway with N_2* hydrogenation as RDS and (c) associative pathway with NNH* dissociation as RDS. (d) The rate expressions for different reaction mechanisms.

Supplementary Notes

The elementary reactions for dissociation pathway and associative pathway are shown in **Table S2** and **Table S3**. We established the kinetic models from different reaction mechanisms based on rate-determining step assumptions.

- **Dissociation pathway & N_2* dissociation as RDS**

The reaction rate can be determined by:

$$r = k_3 \theta_{N_2} \theta_v \tag{S10}$$

With H_2 dissociative adsorption and N_2 adsorption in equilibrium, the surface coverage of N_2* and H* can be determined by:

$$\theta_{N_2} = K_1 p_{N_2} \theta_v \tag{S11}$$

$$\theta_H = \sqrt{K_2 p_{H_2}} \theta_v \tag{S12}$$

As the summary of surface coverage is 1, the surface empty site can be determined by:

$$1 = \theta_v + \theta_{N_2} + \theta_H = \theta_v + K_1 p_{N_2} \theta_v + \sqrt{K_2 p_{H_2}} \theta_v \tag{S13}$$

$$\theta_v = \frac{1}{1 + K_1 p_{N_2} + \sqrt{K_2 p_{H_2}}} \tag{S14}$$

The reaction rate expression can be written as follows.

$$r = \frac{k_3 K_1 p_{N_2}}{(1 + K_1 p_{N_2} + \sqrt{K_2 p_{H_2}})^2} \tag{S15}$$

- **Associative pathway & N_2* hydrogenation as RDS**

The reaction rate can be determined by:

$$r = k_3 \theta_{N_2} \theta_H \tag{S16}$$

With H_2 dissociative adsorption and N_2 adsorption in equilibrium, the surface coverage of N_2* and H* can be determined by Equation (S11) and (S12). As the summary of surface coverage is 1, the surface empty site can be determined Equation (S14). The reaction rate expression can be written as follows.

$$r = \frac{k_3 K_1 p_{N_2} \sqrt{K_2 p_{H_2}}}{(1 + K_1 p_{N_2} + \sqrt{K_2 p_{H_2}})^2} \tag{S17}$$

- **Associative pathway & NNH* dissociation as RDS**

The reaction rate can be determined by:

$$r = k_4 \theta_{\mathrm{NNH}} \theta_v \tag{S18}$$

With H_2 dissociative adsorption, N_2 adsorption and N_2* hydrogenation in equilibrium, the surface coverage of N_2* and H* can be determined by Equation (S11) and (S12), and the surface coverage of NNH* can be determined by:

$$\theta_{\mathrm{NNH}} = K_3 \frac{\theta_{\mathrm{N_2}} \theta_{\mathrm{H}}}{\theta_v} = K_1 K_3 p_{\mathrm{N_2}} \sqrt{K_2 p_{\mathrm{H_2}}}\, \theta_v \tag{S19}$$

As the summary of surface coverage is 1, the surface empty site can be determined by:

$$1 = \theta_v + \theta_{\mathrm{N_2}} + \theta_{\mathrm{H}} + \theta_{\mathrm{NNH}} = \theta_v + K_1 p_{\mathrm{N_2}} \theta_v + \sqrt{K_2 p_{\mathrm{H_2}}}\, \theta_v + K_1 K_3 p_{\mathrm{N_2}} \sqrt{K_2 p_{\mathrm{H_2}}} \tag{S20}$$

$$\theta_v = \frac{1}{1 + K_1 p_{\mathrm{N_2}} + \sqrt{K_2 p_{\mathrm{H_2}}} + K_1 K_3 p_{\mathrm{N_2}} \sqrt{K_2 p_{\mathrm{H_2}}}} \tag{S21}$$

The reaction rate expression can be written as follows.

$$r = \frac{k_4 K_1 K_3 p_{\mathrm{N_2}} \sqrt{K_2 p_{\mathrm{H_2}}}}{(1 + K_1 p_{\mathrm{N_2}} + \sqrt{K_2 p_{\mathrm{H_2}}} + K_1 K_3 p_{\mathrm{N_2}} \sqrt{K_2 p_{\mathrm{H_2}}})^2} \tag{S22}$$

S7 Steady-state Isotopic Transient Kinetic Analysis (SSITKA)

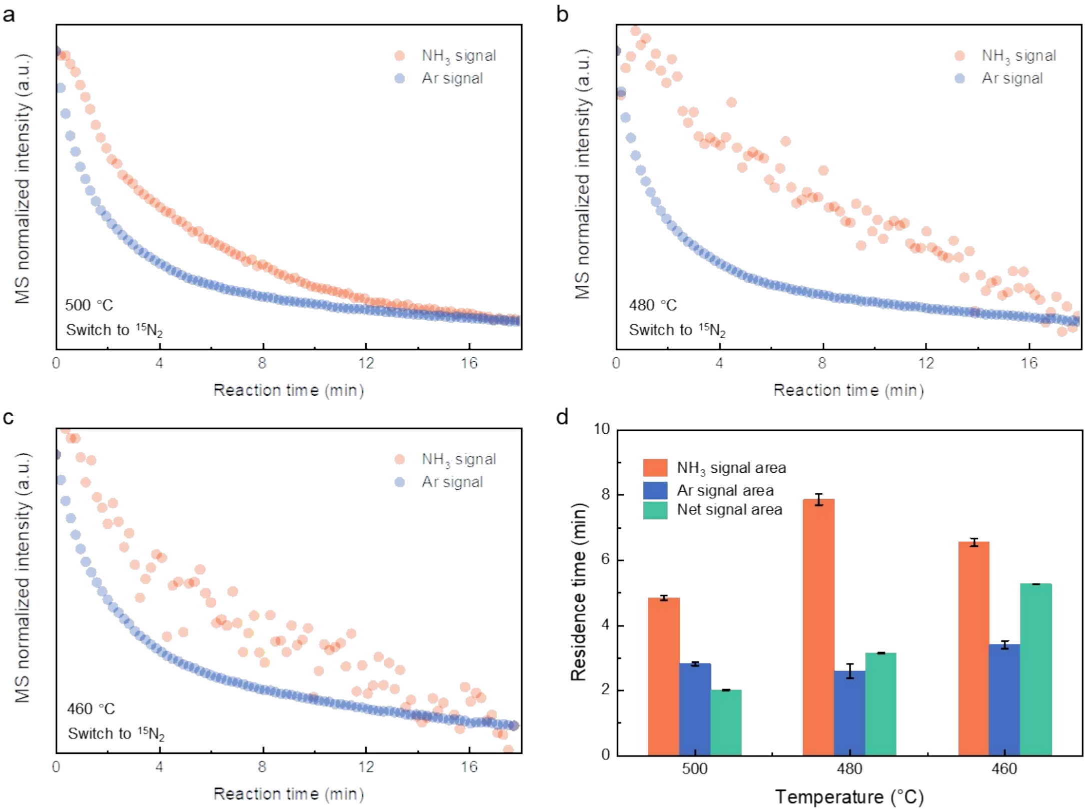

Figure S29 $^{14}NH_3$-$^{15}NH_3$ product signals during the switch process of SSITKA studies under (a) 500 °C, (b) 480 °C and (c) 460 °C. (d) The residence time for different temperatures based on SSITKA.

Supplementary Notes

Steady-State Isotopic Transient Kinetic Analysis (SSITKA) can help us to obtain valuable information on catalyzed heterogeneous reactions at molecular level, including reaction intermediates concentration, site coverage, reactivity, and rate constants[18–20]. The transient responses are recorded and monitored by a mass spectrometer (MS). For a given reversible heterogeneous catalytic reaction at steady-state, a reactant (R) is transformed into a product (P) through an adsorbed intermediate (X). The overall residence time of the product is obtained by the integration of the normalized transient response:

$$\tau_p = \int_0^\infty F_p(t)dt \tag{S23}$$

Using the same method, the residence time of the inert gas can be obtained:

$$\tau_i = \int_0^\infty F_i(t)dt \tag{S24}$$

The net residence time can be obtained:

$$\tau = \tau_p - \tau_i \tag{S25}$$

The reciprocal of the residence time of the intermediate species can be approximated as the turnover frequency (TOF) for intermediate species, which follows the Arrhenius equation. Therefore, the intrinsic activation energy of the rate-determining step can be obtained.

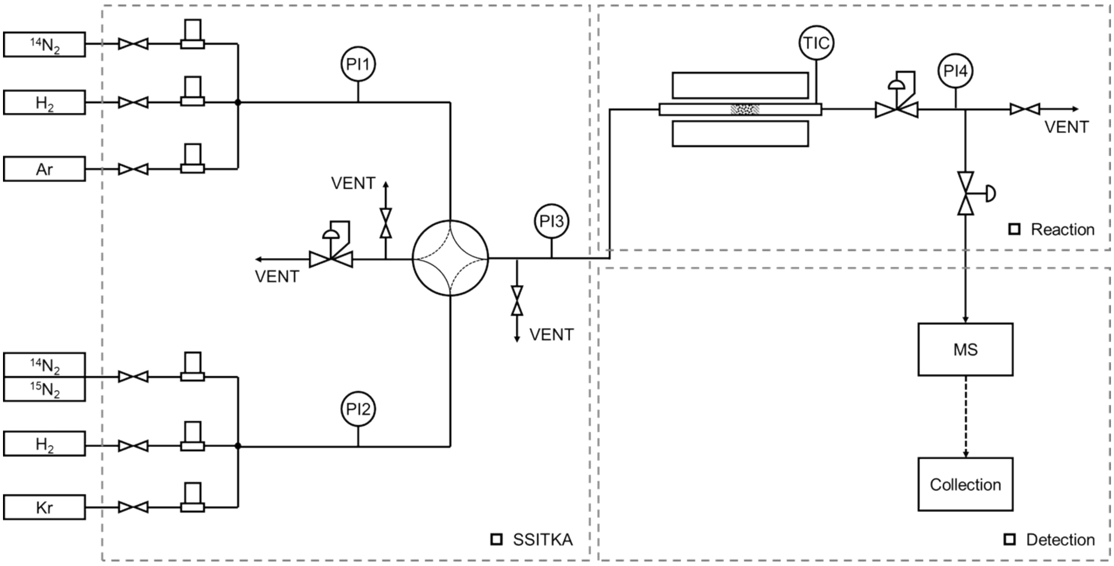

Figure S30 Schematic depiction of SSITKA setup.

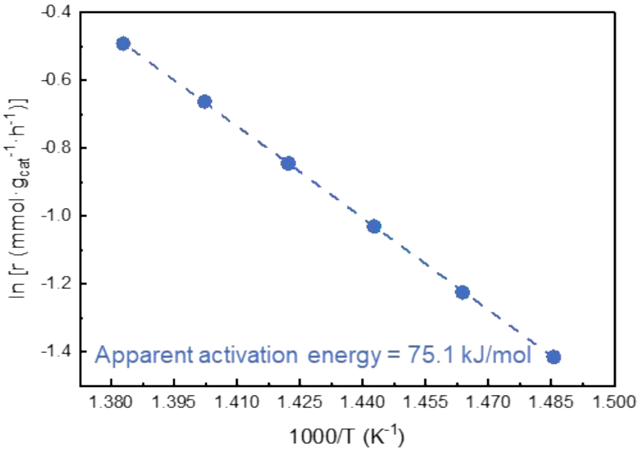

Figure S31 Arrhenius-type plot for steady-state ammonia synthesis.

References

1 G. Kresse and J. Furthmüller, *Comput. Mater. Sci.*, 1996, **6**, 15–50.

2 S. Grimme, S. Ehrlich and L. Goerigk, *J. Comput. Chem.*, 2011, **32**, 1456–1465.

3 G. Kresse and J. Furthmüller, *Phys. Rev. B*, 1996, **54**, 11169–11186.

4 G. Kresse and D. Joubert, *Phys. Rev. B*, 1999, **59**, 1758–1775.

5 J. P. Perdew, K. Burke and M. Ernzerhof, *Phys. Rev. Lett.*, 1996, **77**, 3865–3868.

6 C. D. Zeinalipour-Yazdi, J. S. J. Hargreaves and C. R. A. Catlow, *J. Phys. Chem. C*, 2015, **119**, 28368–28376.

7 C. D. Zeinalipour-Yazdi, J. S. J. Hargreaves and C. R. A. Catlow, *J. Phys. Chem. C*, 2016, **120**, 21390–21398.

8 C. D. Zeinalipour-Yazdi, J. S. J. Hargreaves and C. R. A. Catlow, *J. Phys. Chem. C*, 2018, **122**, 6078–6082.

9 G. Henkelman and H. Jónsson, *J. Chem. Phys.*, 1999, **111**, 7010–7022.

10 D. Sheppard, R. Terrell and G. Henkelman, *J. Chem. Phys.*, 2008, **128**, 134106.

11 R. F. W. Bader, *Acc. Chem. Res.*, 1985, **18**, 9–15.

12 M. Yu and D. R. Trinkle, *J. Chem. Phys.*, 2011, **134**, 064111.

13 C. T. Campbell, *Top. Catal.*, 1994, **1**, 353–366.

14 C. T. Campbell, *J. Catal.*, 2001, **204**, 520–524.

15 C. T. Campbell, *ACS Catal.*, 2017, **7**, 2770–2779.

16 P. Wang, F. Chang, W. Gao, J. Guo, G. Wu, T. He and P. Chen, *Nat. Chem.*, 2017, **9**, 64–70.

17 Q. Wang, J. Pan, J. Guo, H. A. Hansen, H. Xie, L. Jiang, L. Hua, H. Li, Y. Guan, P. Wang, W. Gao, L. Liu, H. Cao, Z. Xiong, T. Vegge and P. Chen, *Nat. Catal.*, 2021, **4**, 959–967.

18 R. H. Nibbelke, J. Scheerova, M. H. J. M. Decroon and G. B. Marin, *J. Catal.*, 1995, **156**, 106–119.

19 S. L. Shannon and J. G. Goodwin, *Chem. Rev.*, 1995, **95**, 677–695.

20 L. M. Aparicio, *J. Catal.*, 1997, **165**, 262–274.